X-ray-absorption near-edge structure of $CuGaSe_2$ and ZnSe: Experiment and theory

O. Šipr, P. Machek, A. Šimůnek, and J. Vackář
Institute of Physics, Academy of Sciences of the Czech Republic, Cukrovarnická 10, 162 00 Praha 6, Czech Republic

J. Horák
University of Pardubice, Náměstí Československých legií , 532 10 Pardubice, Czech Republic
(Received 16 April 1997)

X-ray-absorption near-edge structure (XANES) spectra of a ternary semiconductor $CuGaSe_2$ at the Cu, Ga, and Se edges were measured and compared with Zn and Se spectra of ZnSe, taken from the literature. Having all five absorbing atoms in nearly identical coordination environments, we investigate the influence of the electronic structure on the XANES spectra. The spectra of $CuGaSe_2$ and of ZnSe were calculated using a real-space multiple-scattering approach and using a pseudopotential band-structure technique. Both computational methods yield spectra that are in a good agreement with experiment. The effect of the size of the cluster involved in the real-space calculation on the calculated XANES spectra is investigated. Using self-consistent muffin-tin potentials does not lead to significantly different $CuGaSe_2$ spectra than using non-self-consistent potentials. Real-space multiple-scattering spectra calculated without core holes exhibit only minor differences with respect to those obtained for relaxed screened core holes, the largest effect being found for Zn spectrum of ZnSe. Employing unrelaxed or unscreened core hole potentials resulted in spectra that did not agree with experiment. Contrary to earlier reports, no effect of charge transfer on the calculated XANES spectra of ZnSe was found. [S0163-1829(97)03744-2]

I. INTRODUCTION

X-ray-absorption spectroscopy (XAS) has established itself as a useful tool for structural studies, especially in systems with broken translation symmetry. There are two ingredients that determine the form of x-ray-absorption spectra: (i) the arrangement of atoms around the absorbing atom and (ii) the electronic structure of the material. It has been known for a long time that the geometrical aspect (''real structure'') dominates in the extended x-ray-absorption fine-structure (EXAFS) region while the electronic structure significance increases in the x-ray-absorption near-edge structure (XANES) region.

Most applications of XAS to structural studies involve EXAFS spectra. In that case, due to the high energy of the excited photoelectron, it is usually sufficient to describe scattering properties of atoms in a solid using basically a free-atom model, neglecting thus the details of the electronic structure completely. The relative straightforward extraction of the structural information from EXAFS data is possible because x-ray-absorption spectra are sensitive to bond lengths only in that region. If information involving bond angles is of interest (e.g., orientation of an adsorbed molecule with respect to the surface), one has to rely on XANES. Then, in contrast to EXAFS, the electronic structure of the investigated material may play an important role. It is therefore crucial to assess the relative importance of the influence of the real structure and of the electronic structure of the compound on its XANES spectrum.

The most straightforward way to separate geometric and electronic-structure related contributions to XANES spectra is to investigate edges of different atoms surrounded by an identical *geometrical* arrangement of atoms. Such a suitable system presents Cu, Ga, and Se *K* edges of a ternary I-III-VI_2 chalcopyrite semiconductor $CuGaSe_2$ and Zn and Se *K* edges of its isoelectronic II-VI analog, ZnSe. As ZnSe crystallizes in a cubic zinc-blende structure and $CuGaSe_2$ forms its nearly perfect supercell (apart from 2% tetragonal distortion and 1% contraction of bond lengths), we have in total five edges of atoms in nearly *identical geometrical environments* to compare. Hence, all differences among these x-ray absorption spectra must be due to electronic structure effects. By comparing analogous spectra in different compounds (Cu, Ga, and Zn edges on the one side, Se edges on the other side), the effect of ''averaging of formal valences'' on the XANES spectra can be investigated as well.

Ternary chalcopyrite semiconductors have been subject to intensive research on their own (also due to their potential technological relevance to photovoltaic solar cells, light-emitting diodes, and nonlinear optical devices). Their electronic structure was theoretically investigated by Jaffe and Zunger.[1] All three *K* edges of $CuFeS_2$ were measured and compared to Cu, Fe, and S spectra of compounds with similar or different atomic arrangements.[2] Experimental sulfur x-ray absorption spectra of ZnS, $CuGaS_2$, and $CuFeS_2$ were analyzed by Sainctavit *et al.*[3] McKeown[4] compared both measured and calculated Cu, Fe, and Zn XANES *K* spectra of $CuFeS_2$ and ZnS.

This paper contains analyses of both experimental and theoretical spectra of all cation as well as anion edges of a ternary semiconductor $CuGaSe_2$ and of its binary analog ZnSe. The experimental spectra of $CuGaSe_2$ were recorded in our laboratory, the experimental spectra of ZnSe were taken from an earlier work of Matsuura, Fujikawa, and Oyanagi.[5] Two methods of calculation of XANES spectra were employed, namely, a pseudopotential band-structure

technique and a real-space multiple-scattering approach. The sensitivity of the calculated spectra to self-consistency in the potential, to the core hole treatment, and to the cation-anion charge transfer is also investigated.

II. EXPERIMENT

$CuGaSe_2$ samples were prepared in the polycrystalline form. The synthesis was performed in a quartz ampoule and Ar atmosphere (the gas pressure about 2 Pa) from elements of $5N$ purity. The stoichiometric melt was gradually heated to 900 °C; at this temperature the melt was held for 18 h. To homogenize the sample, the temperature was raised to 1150 °C and maintained for 6 h, then lowered to 900 °C, held at this temperature for 5 days, and finally cooled.

The Cu, Ga, and Se absorption K edges in $CuGaSe_2$ were measured using a two-crystal spectrometer and an x-ray spectrometry tube. The analyzing crystals were Si(111) and Si(220) in the $(m,-n)$ position. The spectra were collected in a transmission mode. Each measured data point shown here represents an average of repeated measurements. The measured spectra were deconvoluted by the apparatus smearing function.

III. CALCULATIONS

A. Band-structure calculation

For calculating electronic structure and x-ray absorption spectra of $CuGaSe_2$ and ZnSe, a self-consistent pseudopotential approach was employed.[6] The atomic pseudopotentials were generated by the phase-shift technique,[7] the Ceperley-Adler exchange, and a correlation term in an analytical form[6] was used.

The potentials permitted tractable computation in a plane-wave basis with a cutoff in kinetic energy of 30 Ry for structures having eight atoms in a unit cell. While this imposes no restraints on ZnSe, the real $CuGaSe_2$ compound with 16 atoms per unit cell cannot be treated in this way. Therefore, instead of a full $CuGaSe_2$ geometry, a simplified structure was dealt with (see Tables I and II and Fig. 1). In this simplified structural model, the local structure around all atoms in $CuGaSe_2$ is preserved, only positions of atoms forming second-nearest neighbors are interchanged compared to the full structure of the real $CuGaSe_2$. The crystallographic data necessary for our work were taken from the CRYSTIN database.[8]

For the calculation of the x-ray transition matrix element, the radial part of it is approximated by a constant in the whole energy range of spectra. The angular part of the matrix element was calculated exactly, using the plane-wave basis mentioned above. The calculated K-spectra have been convoluted with a Lorentzian function to take into account the lifetimes of the $1s$ core holes. More details about the computational technique are given in Ref. 9.

B. Real-space multiple-scattering approach

The principles of the real-space multiple-scattering (RS-MS) approach were thoroughly reviewed elsewhere.[10,11] The computer code we used is an amended version of the ICXANES program of Vvedensky, Saldin, and Pendry.[12] Their approach makes it possible to handle even very large clusters of atoms by dividing the whole cluster into shells and calculating the scattering within individual shells and between them separately. In all real-space calculations presented here, full multiple scattering was taken into account. The maximum angular momentum included in the single-site scattering was $\ell_{max}=4$; the maximum angular momentum included in the intershell scattering[13] was $\ell_{out}=20$. Both of these limits were checked for convergence.

TABLE I. Unit cell axes and positions of atoms inside a unit cell of real $CuGaSe_2$. Positions of atoms are in Cartesian coordinates. All lengths are in angströms.

		$CuGaSe_2$—full geometry		
Lattice vectors:	a	5.61	0.00	0.00
	b	0.00	5.61	0.00
	c	0.00	0.00	11.00
Atoms:	Cu	0.00	0.00	0.00
	Cu	0.00	2.80	2.75
	Cu	2.80	2.80	5.50
	Cu	2.80	0.00	8.24
	Ga	2.80	2.80	0.00
	Ga	2.80	0.00	2.75
	Ga	0.00	0.00	5.50
	Ga	0.00	2.80	8.24
	Se	1.40	1.40	1.37
	Se	4.21	4.21	1.37
	Se	1.40	4.21	4.12
	Se	4.21	1.40	4.12
	Se	4.21	4.21	6.87
	Se	1.40	1.40	6.87
	Se	4.21	1.40	9.62
	Se	1.40	4.21	9.62

1. Construction of muffin-tin potential

The RS-MS approach relies on the so-called muffin-tin approximation, which considers the crystal potential to be spherically symmetric inside nonintersecting spheres around individual atoms and constant in the interstitial region. Both

TABLE II. Unit cell axes and positions of atoms inside a unit cell of a simplified $CuGaSe_2$. Positions of atoms are in Cartesian coordinates. All lengths are in angstroms.

		$CuGaSe_2$—simplified geometry		
Lattice vectors:	a	5.61	0.00	0.00
	b	0.00	5.61	0.00
	c	0.00	0.00	5.50
Atoms:	Cu	0.00	0.00	0.00
	Cu	0.00	2.80	2.75
	Ga	2.80	2.80	0.00
	Ga	2.80	0.00	2.75
	Se	1.40	1.40	1.37
	Se	4.21	4.21	1.37
	Se	1.40	4.21	4.12
	Se	4.21	1.40	4.12

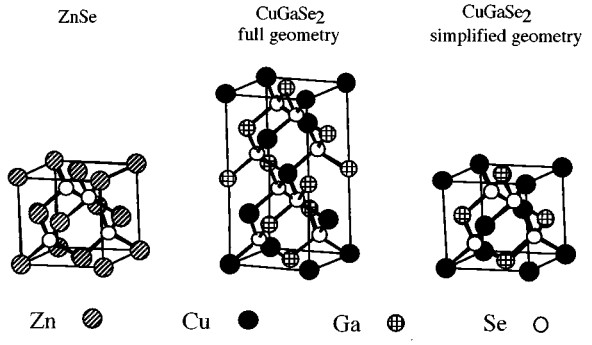

FIG. 1. Perspective diagrams of unit cells of ZnSe and $CuGaSe_2$ and of the simplified version of $CuGaSe_2$.

non-self-consistent and self-consistent potentials were tested in our real-space calculations.

A standard way of constructing a non-self-consistent muffin-tin potential is via the Mattheiss prescription:[14] electron densities calculated for free atoms are put in appropriate positions of the crystal lattice and Coulombic (Hartree) and exchange parts of the crystal potential are calculated as superpositions of partial contributions from individual atoms. This type of potential proved to be very useful in XANES calculations in the past[15] and we employed it here as well.

Electron densities for free atoms were calculated self-consistently, making use of the local density approximation. The exchange-correlation potential of Ceperley and Adler[6] was used for atomic calculations. In constructing the Mattheiss potential appropriate for unoccupied states, the energy-independent $X\alpha$ potential with the Kohn-Sham value of $\alpha=0.66$ was used.[16]

A self-consistent muffin-tin potential was constructed for $CuGaSe_2$ using the results of pseudopotential band-structure calculations. The electron charge density within spheres of radius $R_S=2.50$ a.u. around each atom was reconstructed from self-consistent pseudodensities via the procedure described in Ref. 17, and the electron density in the space between those spheres was simply identified with the pseudodensity. The electron density obtained in this way was then distributed among particular atoms according to the ''Wigner-Seitz'' criterion (every point of a crystal was attributed to the atom that was the closest one to it) and made spherically symmetric by angular averaging. This partitioning of the self-consistent electron charge makes it possible to construct a self-consistent muffin-tin potential via the same technical procedures as in the case of the Mattheiss potential.

We used nonoverlapping spheres, and the muffin-tin radii were determined so that the initial superimposed potentials matched at the touching points (or rather, as this condition cannot be strictly met for all atoms, so that the overall potential difference is as small as possible). The muffin-tin zero was set to the average interstitial potential. This procedure introduces a step in the potential at the sphere boundaries, which may occasionally lead to unphysical oscillations in the XANES spectra.[18] However, on the average such a potential deviates from the ''true'' non-muffin-tin potential less than it does in the case when the muffin-tin zero is identified with the value of the intrasphere potential at the sphere boundary.

To check whether our results are sufficiently robust with respect to small changes in the somewhat arbitrary muffin-tin parameters, we made a few exploratory calculations for different choices of muffin-tin zero (reducing thus the potential step at the sphere boundaries) for different sets of muffin-tin radii and also introducing a 20% sphere overlap. No significant changes in the spectra were observed.

2. Treatment of core hole

The transition of an electron from a deep core level into unoccupied orbitals is an intrinsically dynamic process, as all other electrons tend to react to the creation of a hole left behind. At least in certain classes of materials, however, this process can be described in terms of transitions between single-particle states of a static Hamiltonian. In simple metals, the ''final-state rule'' has been proven,[19] according to which the states of the excited photoelectron ought to be calculated in a static potential that takes into account the presence of a core hole. On the other hand, Stern and Rehr[20] investigated the x-ray absorption process using a reformulated Hartree-Fock approach and found that it reduces to a single-particle problem only in the limits of transitions to nearly empty and nearly filled bands: in the former case the final state with a core hole is the appropriate one, while in the latter case the ground-state potential (without core hole) ought to be used.

Currently, there seems to be no sufficiently general and simple rule available to estimate, without explicit calculation, whether the core hole effect is significant for a particular XANES spectrum or not. Self-consistent electronic structure calculations demonstrated that the significance of the core hole for XANES spectra simulation strongly depends on the type of the edge and on the material considered.[21,22] Indeed, in some cases, the presence of a core hole has no significant effect on the x-ray absorption spectra,[23–25] while in other cases it was found to be important and possible to be taken into account via the final-state rule.[26,27] Thorough studies of bcc metals[28] and of transition-metal disilicides[29,30] found that neither neglecting the core hole altogether nor taking it into account (relaxed and screened by passive electrons) resulted in a fully satisfactory agreement between measured and calculated XANES spectra.

More types of ''core hole potentials'' can be introduced, depending on the way the remaining (passive) electrons are allowed to respond to the occurrence of a hole in an inner atomic shell. To investigate the core hole effect in I-III-VI_2 and II-VI semiconductors, we considered the following options: (i) ground-state potential (no core hole), (ii) relaxed and screened core hole (atomic calculation performed for a 1*s* vacancy and one extra electron added to the lowest unoccupied level), (iii) relaxed unscreened core hole (atomic calculation performed for an atom with a 1*s* vacancy, i.e., for a ion), and (iv) unrelaxed unscreened core hole (atomic calculation was performed for a ground-state atom and the 1*s* electron was removed only afterwards). The frequently used ''$Z+1$'' approximation corresponds to our second option (relaxed passive electrons and screened core hole).

3. Charge transfer

When constructing non-self-consistent potentials appropriate for XANES calculations of partially ionic compounds, there is a question of how to simulate the effect of the elec-

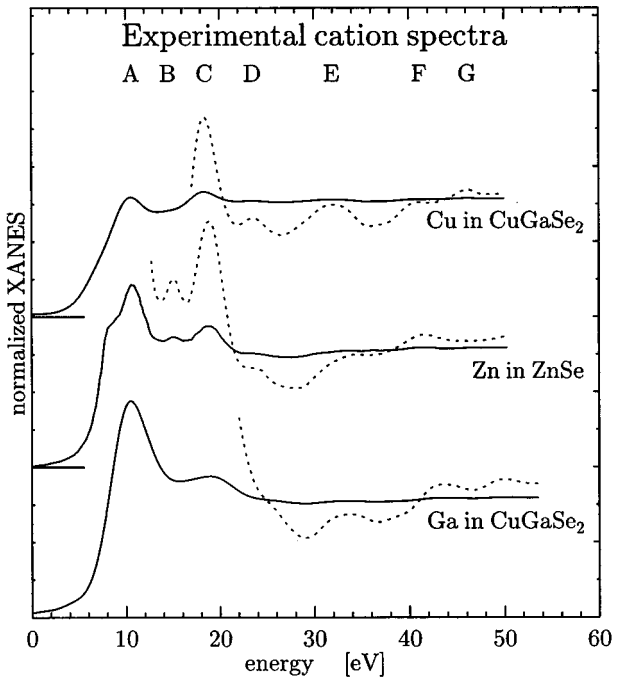

FIG. 2. Experimental K-edge spectra of Cu and Ga in $CuGaSe_2$ and of Zn in ZnSe. Dotted lines are experimental curves multiplied by ten. The ZnSe spectrum is taken from Ref. 5.

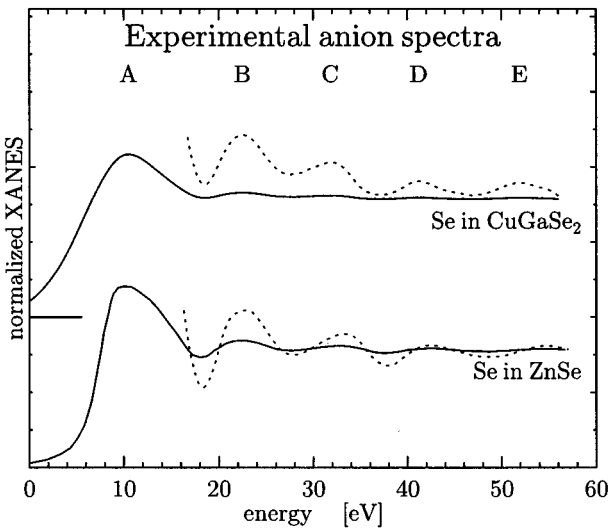

FIG. 3. Experimental K-edge spectra of Se in $CuGaSe_2$ and of Se in ZnSe. Dotted lines are experimental curves multiplied by ten. The ZnSe spectrum is taken from Ref. 5.

tron charge transfer between the cation and the anion. Contradictory conclusions were reached in the past concerning the necessity to consider such processes for accurate x-ray-absorption spectra calculations (compare Refs. 5,31 and 32–34). As an earlier work on ZnSe reported a significant sensitivity of XANES spectra to the charge distribution,[5] we included the investigation of this effect to our study as well.

We compare results obtained with *no electron charge redistribution* and with a charge redistribution predicted by the *Pauling electronegativity model*. In the latter case, the amount of the redistributed charge q associated with the A–B bond of an $A^N B^{8-N}$ crystal with a coordination number M is[35]

$$q = 1 - \frac{N}{M} \exp\left[-\frac{1}{4}(X_A - X_B)^2 \right], \tag{1}$$

where X_A and X_B are Pauling electronegativities of elements A and B. For ZnSe, this method yields a charge distribution $Zn^{0.57}Se^{-0.57}$. For $CuGaSe_2$, after using the average electronegativity of Cu and Ga for X_A and splitting the total cation charge between Cu and Ga in a 1:3 ratio, we get $Cu^{0.27}Ga^{0.83}Se_2^{-0.55}$.

IV. RESULTS AND DISCUSSION

A. Experimental cation and anion spectra

Our experimental results for $CuGaSe_2$ are presented in Figs. 2 and 3, together with ZnSe experimental data of Matsuura *et al.*[5] All spectral curves have been normalized so that they would have the same height at the high-energy tail (this is true also for all theoretical curves presented in this paper). The horizontal alignment between different spectra was chosen to achieve the best possible overall agreement between corresponding peaks of different spectra. The origin of the energy scale is arbitrary.

The spectra split naturally into two classes—cation spectra and anion spectra. Note that although the geometrical arrangements of atoms are identical when ''seen'' from either cation or anion sites, the differences between XANES spectra are resolvable at first sight for the two groups.

Spectra of ZnSe and of $CuGaSe_2$ can be compared with analogous spectra of chemically and structurally similar compounds: McKeown[4] presents K-spectra of Zn in ZnS and of Cu and Fe in $CuFeS_2$, experimental K-spectra of sulfur in ZnS, $CuGaS_2$, and $CuFeS_2$ can be found in Ref. 3, and Zn K-edge and Te L_1-edge spectra of ZnTe are shown in Ref. 36. Indeed, when rescaling due to different lattice constants is taken into account, gross features of the cation spectra mentioned above correspond to spectra displayed in Fig. 2, while the sulfur spectra[3] resemble spectra shown in Fig. 3. Interestingly, the Te L_1 edge of ZnTe does not quite fit into this scheme—maybe because of different matrix elements for K and L_1-edge spectra.

Our main concern, however, is comparison of ZnSe and $CuGaSe_2$ spectra. There are differences not only between the cation spectra on the one side and the anion spectra on the other but also among particular spectra within each group. The differences between Cu, Zn, and Ga spectra (Fig. 2) are larger than between Se spectra of $CuGaSe_2$ and ZnSe (Fig. 3). This indicates that the central atom (i.e., the atom with the core hole) has an important role in the formation of the XANES spectrum. This is consistent with the conclusion of McKeown[4] that the edge shapes of Zn in ZnS and of Cu and Fe in $CuFeS_2$ are determined mainly by atomiclike factors.

The height of the first peak of cation spectra (labeled A in Fig. 2) increases in the order $Cu^{I} \rightarrow Zn^{II} \rightarrow Ga^{III}$, contrary to the $Fe^{III} \rightarrow Cu^{I} \rightarrow Zn^{II}$ sequence in $CuFeS_2$ (Ref. 4). There are no prepeaks at any edge of $CuGaSe_2$ (note that a preedge feature appears at the Cu edge for most copper compounds[2]). The Zn spectrum shows some details in the near-edge region

that are not observed in the Cu or Ga edge of $CuGaSe_2$, although there are no significant differences among Cu, Zn, and Ga core hole lifetimes.[37] It is evident from Fig. 2 that the Zn spectrum definitely is *not an average* of Cu and Ga spectra, as one might naively expect by judging just from their isoelectronic analogy.

The most visible difference between Se spectra of the two compounds (Fig. 3) is that the intensity at the low-energy side of the main peak *A* is higher for $CuGaSe_2$ than for ZnSe. This is in agreement with the analogous situation for $CuGaS_2$ and ZnS (Ref. 3)—one just has to keep in mind differences in core hole lifetime broadenings of S and Se K spectra (0.59 eV vs 2.33 eV, according to Ref. 37).

B. Band-structure calculation

The band structure of $CuGaSe_2$ was at first used for calculation of *K* emission bands of all three elements. A very good agreement between theoretical and experimental x-ray-emission spectra was found.[38] In this paper we applied the self-consistent band-structure results to unoccupied states. The outcome is presented in Fig. 4. (Note that the origin of the energy scale coincides with the computed top of the valence band of $CuGaSe_2$ in all graphs of this figure.) As can be seen, the theory reproduces the experiment very well, particularly in the near-edge region (up to 20 eV above the onset of the conduction band).

XANES spectra of ZnSe were calculated in this way as well, with the agreement between theory and experiment being similar to that for $CuGaSe_2$. As this ''reference compound'' is not in our focus in this work, the results will be presented only together with the outcome of real-space calculations in Sec. V.

C. Cluster size effect

The real-space approach makes it possible to estimate the spatial extent of the region where particular spectral features are ''formed.'' To facilitate contact with band-structure calculation, we performed the cluster size analysis for the potential reconstructed from selfconsistent pseudopotentials, as described in Sec. III B 1. As $CuGaSe_2$ and ZnSe spectra provided basically the same picture for the dependence of XANES spectra on the cluster size, only $CuGaSe_2$ results are summarized in Fig. 5. No broadening of the spectral curves was introduced at this stage. In Table III, details about the first ten ZnSe coordination spheres and their $CuGaSe_2$ counterparts are provided. Two or three atomic shells were always joined into a single shell for the purpose of our shell-by-shell multiple-scattering calculations (see Sec. III B).

The general conclusion that can be made from Fig. 5 is that while high and distinct peaks are reproduced within relatively small clusters, very large clusters are necessary to be involved if correct simulation of fine spectral details is required: the principal peaks (denoted *A* and *C* for cation and *A* and *B* for anion spectra) are typically reproduced within 17-atoms clusters, very small peaks (D, F, and G for cations and C and D for anions) appear distinctly at their converged positions only for clusters including more than 200 atoms. A similar conclusion for Ba edges of BaF_2 could be drawn from recent results of Chaboy.[39]

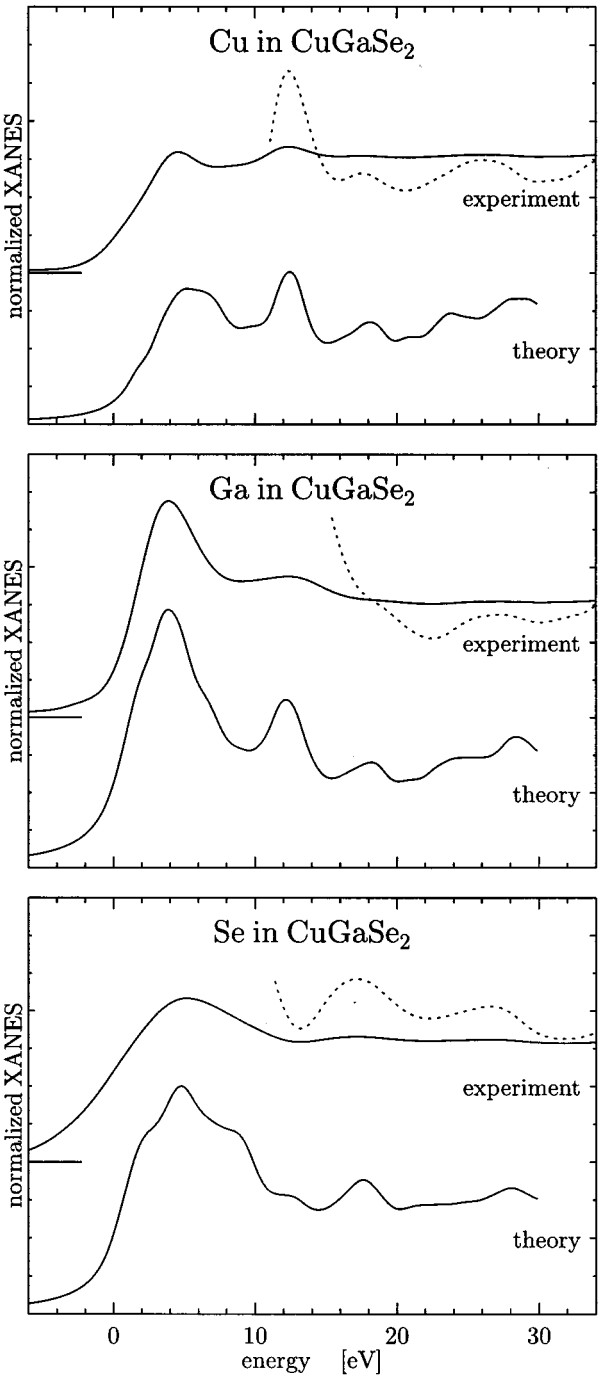

FIG. 4. Results of pseudopotential band-structure calculation of Cu, Ga, and Se *K*-edges of $CuGaSe_2$ together with the experiment. The zero energy corresponds to the bottom of the conduction band. Dotted lines are experimental curves multiplied by ten.

A fairly well cluster-size-converged $CuGaSe_2$ spectrum can be obtained for 47 atoms. Not surprisingly, this is also the cluster size that McKeown[4] found sufficient for the $CuGaSe_2$ spectra calculation. Note that just five atoms are usually not sufficient to describe prominent peaks at the edges satisfactorily.

Another feature worth attention is that the ''fine structure'' at the low-energy side of the main peak *A* in the Se spectrum appears only for clusters containing at least 71 at-

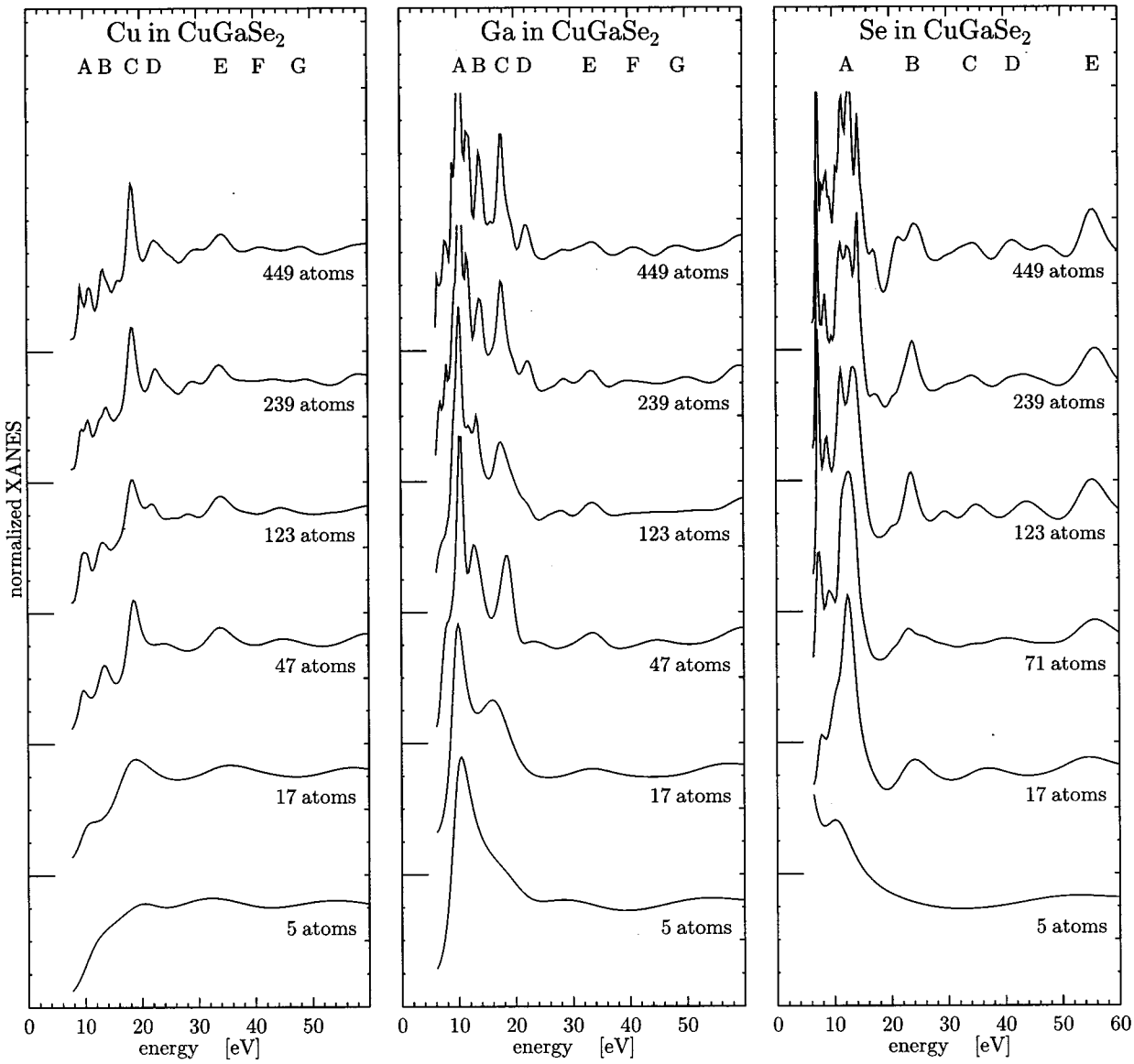

FIG. 5. Real-space multiple-scattering calculation of XANES spectra of $CuGaSe_2$ for a few representative cluster sizes. Muffin-tin potential constructed from self-consistent band-structure calculation used, core hole not taken into account. The origin of the energy scale is arbitrary.

oms. This, together with the fact that at least 47 atoms are needed to reproduce the kink at the low-energy side of the *A* peak in Zn spectrum of ZnSe (results not displayed here for brevity—cf. Fig. 2 and Sec. IV F below), relates to the discussion of whether prepeaks and features at the very edge ought to be attributed to atomic bound-state transitions of the absorber or whether they can be ascribed to interference effects from crystal structure (compare, e.g., Ref. 2 with Ref. 4 for $CuFeS_2$ or Ref. 40 with Ref. 41 for copper oxides): the common experience is that, usually, preedge features can be reproduced by RS-MS calculations provided sufficiently large clusters are taken into account. However, precisely in this preedge energy region (i.e., close to the muffin-tin zero), the drawbacks of the muffin-tin approximation and of the usual non-self-consistency in scattering potentials are expected to be most serious. It seems, therefore, that more research is needed before definite conclusions about this issue can be made.

TABLE III. Atomic shells in $CuGaSe_2$ and ZnSe: number of atoms in a particular shell, cumulative numbers of atoms in all lower shells including the one in concern, distances of atoms of given shell from the absorbing atom (in angströms).

Shell label	No. of atoms in the shell	Cumulative no. of atoms	Distances in $CuGaSe_2$	Distance in ZnSe
1	1	1	0.00	0.00
2	4	5	2.41	2.43
3	12	17	3.93,3.96	3.97
4	12	29	4.57,4.60	4.66
5	6	35	5.49,5.61	5.62
6	12	47	6.05,6.10	6.12
7	24	71	6.77,6.84	6.88
8	16	87	7.15,7.23,7.28	7.30
9	12	99	7.85,7.93	7.94
10	24	123	8.22,8.25,8.29	8.31

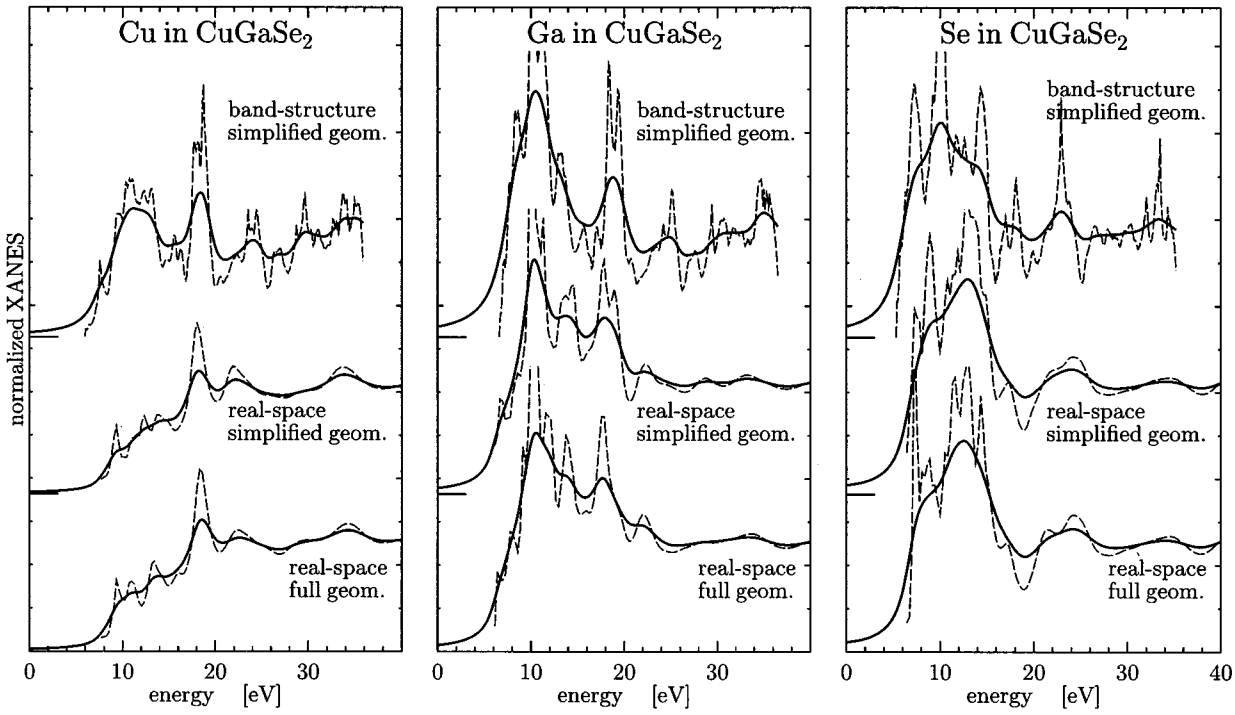

FIG. 6. XANES spectra of $CuGaSe_2$ calculated using the band-structure technique for an infinite solid and applying the RS-MS formalism for a 449-atomic cluster. Band-structure spectra were calculated for the simplified $CuGaSe_2$ geometry only (cf. Sec. III A and Fig. 1), real-space spectra are presented both for the simplified and for the full geometry. Solid lines represent results that were smoothed to account for finite core-hole lifetimes, broken lines stand for nonsmoothed spectra.

D. Comparison of real-space multiple-scattering and band-structure calculations

In the preceding section, we studied how $CuGaSe_2$ spectra evolve when the cluster size is being increased up to 449 atoms (radius of such a cluster is 13.1 Å). The next logical step is to investigate theoretical spectra for infinitely large clusters, i.e., relying on band-structure methods. Comparison of band-structure spectra with real-space spectra of 449-atom clusters is done in Fig. 6. The same crystal potentials were used in both approaches (apart from the muffin-tin constriction in the RS-MS case). Both ''raw'' spectra as well as spectra convoluted with Lorentzian curves to account for core hole lifetimes[37] are presented. As the band structure was calculated for a simplified model $CuGaSe_2$ geometry (cf. Sec. III A), real-space results are presented both for a full and for a simplified geometry as well. The origin of the energy scale in Fig. 6 as well as the horizontal alignment of band-structure and RS-MS spectra are arbitrary.

The first conclusion to be reached from comparing the corresponding real-space curves in Fig. 6 with each other is that simplifying the $CuGaSe_2$ geometry as in Sec. III A does not effect the resulting x-ray spectra significantly. Another striking feature revealed by Fig. 6 is that while for Ga and Se spectra both band-structure and RS-MS approaches yield very similar results, there are large differences for the Cu edge in the low-energy region (for $E<15$ eV).

It is not quite clear what is the origin of this discrepancy. It cannot be due to the finite size of the cluster, as convergence with respect to cluster size was reached for as few as 47 atoms in this energy region (cf. Fig. 5). Hence, just two sources of disagreement are left: either omission of the energy dependence of the radial parts of band-structure matrix elements (see Sec. III A) or neglect of non-muffin-tin effects in the RS-MS calculation. The good agreement between the band-structure Cu spectrum and the experiment, as seen from Fig. 4, suggests that omission of the energy-dependence of matrix elements is a reasonable approximation in this case. Therefore, the most probable explanation for the disagreement between band-structure and real-space results for the Cu edge seems to be the neglect of non-muffin-tin effects in our RS-MS approach. To our knowledge, this is for the first time that a failure of the muffin-tin approximation in calculating XANES spectra of solids is indicated by comparing muffin-tin and non-muffin-tin calculations (for molecules, this was done by Foulis, Pettifer, and Sherwood[42]). Clearly, a more detailed analysis of this subject is still needed.

Another interesting point to note when comparing non-smoothed band-structure and real-space curves in Fig. 6 is that the agreement between the two calculations is better for lower energies than for higher ones: peaks at band-structure curves are significantly sharper than peaks at real-space curves for $E>20$ eV, although for lower energies the shapes of peaks are quite similar both for band-structure and real-space spectra. A similar tendency can be seen, e.g., in KCl band-structure and RS-MS spectra of Datsyuk, Gegusin, and Vedrinskii[43] (although for a much smaller cluster of 57 atoms).

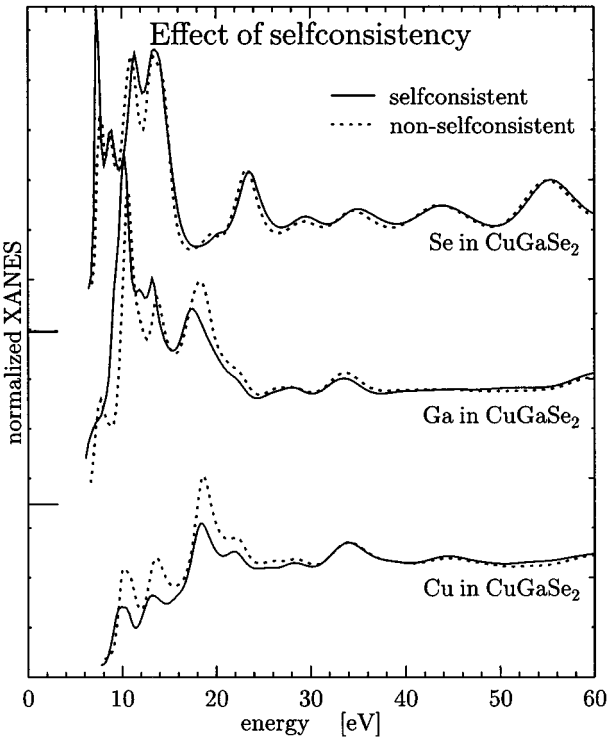

FIG. 7. RS-MS calculation of Cu, Ga, and Se spectra of $CuGaSe_2$ for a cluster of 123 atoms for a muffin-tin potential taken from self-consistent band-structure calculation (solid line) and for non-self-consistent potential constructed via the Mattheiss prescription (dotted line). The core hole is not included in either case.

E. Sensitivity to the scattering potential construction

1. Effect of self-consistency

All RS-MS curves presented so far were calculated using a self-consistent muffin-tin potential obtained from a pseudopotential band-structure calculation. As most XANES calculations rely on the non-self-consistent Mattheiss potential, is may be useful to test quantitatively its suitability for a nontrivial semiconducting compound. Therefore, for each of the three $CuGaSe_2$ edges, we performed two ''identical'' RS-MS calculations using the same cluster of 123 atoms but two different potentials. The differences between XANES spectra generated by a self-consistent and by a non-self-consistent (Mattheiss) potential are demonstrated in Fig. 7. Clearly, both potentials give rise to very similar spectra. This finding is consistent with analogous analysis done earlier, e.g., for insulating CaO by Wille, Durham, and Sterne[33] and for metallic Cu by Šipr, Vackář, and Šimůnek.[44]

Let us stress again that, due to the muffin-tin model involved in our RS-MS calculation , the self-consistent potential investigated in Fig. 7 is not the same as the potential that gives rise to the theoretical spectra calculated by the band-structure technique (Fig. 4). This may be particularly significant at the first ~10 eV of the Cu spectrum. As noted in Sec. IV D, the ''self-consistent'' real-space calculation does not reproduce the experiment in this energy region accurately—rather, it closely resembles non-self-consistent results. This recalls the conclusion of Foulis, Pettifer, and Sherwood[42] that by imposing muffin-tin constraints on the molecular potential, one effectively loses the benefits of self-consistency.

2. Core hole effect

In Sec. III B 2, we reviewed briefly previous investigations of the core hole effect, quoting that (i) its significance may depend strongly on the chemical type of absorbing atom and that (ii) neither neglecting the core hole nor taking it into account results in an accurate description of experimental spectra in some cases. To investigate the core hole effect in $CuGaSe_2$ and ZnSe, we calculated x-ray-absorption spectra for four different models of core hole potentials and compare them with each other and with the experiment (Fig. 8).

Our first finding is that, generally, the best agreement with experiment is found either without any core hole or with a relaxed and screened core hole potential (which is the usual option of how it is dealt with). This agrees well with findings of Gegusin *et al.*[32] for alkali halides and of Chaboy[39] for BaF_2 (note, however, that Tamura *et al.*[21] found that the core hole relaxation is not a complete one for metals). The relaxed and unscreened potential, suggested, e.g., by Refs. 45–47, performs worse than a relaxed and screened one in Fig. 8.

There is no significant difference between curves corresponding to calculations with no core hole and with a relaxed and screened core hole—with the exception of the Zn edge in ZnSe: in that case, a notable increase of the first peak intensity is observed when the core hole is taken into account, thereby improving the agreement between theory and experiment significantly. This supports the general conclusion of Weijs *et al.*[48] that the main effect of a core hole consists in increasing the intensity of the XANES spectrum close to the Fermi energy (this effect is demonstrated clearly also in Refs. 32, 43 and 49).

There seems to be no obvious intuitive reason why the core hole effect should be significant just in the Zn spectrum and not in the others—neither phase shifts nor scattering amplitudes have any anomaly or distinctive feature that would indicate this peculiarity ''in advance.'' Hence, our analysis supports the experience mentioned in Sec. III B 2, viz., that it is not possible to make a qualified judgment about the significance of the core hole effect for a particular XANES spectrum without calculating it.

3. Effect of charge transfer

We investigated the effect or charge transfer on x-ray-absorption spectra of $CuGaSe_2$ and ZnSe by comparing the spectra calculated for a Mattheiss potential generated by neutral atomic charge densities and by charge densities of appropriate ions, as specified in Sec. III B 3. Figure 9 presents comparison of XANES spectra of ZnSe for these two types of potentials. Evidently, hardly any influence of the ionic charges can be seen. Similarly, $CuGaSe_2$ spectra also do not display any dependence on the charge transfer (we do not present the results here for brevity).

There seems to be a direct contradiction of our results with the results of Matsuura, Fujikawa, and Oyanagi,[5] who report a significant sensitivity of their calculated spectra to the amount of ionic charges on the atoms in ZnSe. We are not able to identify the reason for this disagreement. Our confidence in the results presented here follows partially from the good agreement of our calculated spectra with ex-

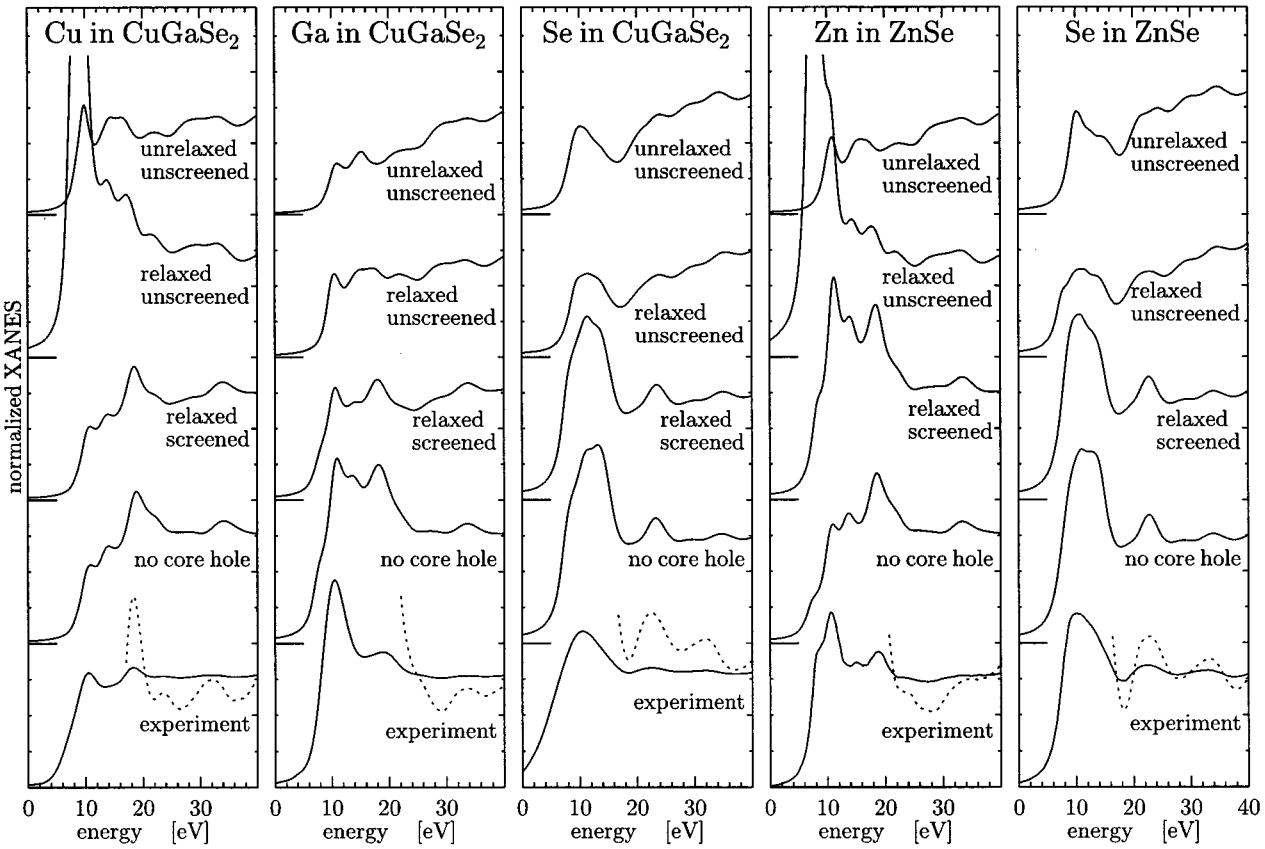

FIG. 8. RS-MS calculation of x-ray-absorption spectra of $CuGaSe_2$ and of ZnSe for a cluster of 123 atoms for different core hole treatments (cf. Sec. III B 2). For comparison, experimental spectra are included as well (experimental curves for ZnSe are taken from Ref. 5). Theoretical curves were smoothed to account for finite core hole lifetimes.

periment (see Sec. IV F), which is considerably better than in the work of Matsuura, Fujikawa, and Oyanagi[5] (probably mainly due to larger cluster sizes employed here).

We conclude, therefore, that there appears to be very little sensitivity of the calculated XANES spectra to the way of dealing with the charge transfer during Mattheiss potential construction.

F. Comparison of theory and experiment

In previous sections, we investigated the influence of various factors on the calculated x-ray-absorption spectra. Here, in Figs. 10 and 11, we finally present a detailed comparison between theory and experiment. Both band-structure as well as RS-MS calculations were performed for $CuGaSe_2$ and ZnSe. The real-space results presented in this section were obtained for clusters of radii 13.2 Å, including 449 atoms for $CuGaSe_2$ and 441 atoms for ZnSe. All theoretical curves were broadened to account for core hole lifetimes but not for experimental apparatus smearing. The relative positions of individual curves with respect to the energy axis were chosen so that the best overall fit between spectral peak positions would be obtained.

For $CuGaSe_2$ spectra, shown in Fig. 10, a real-space calculation was done for the muffin-tin form of the same self-consistent potential as used for calculating the band-structure curves. The presence of a core hole was omitted, as justified in Sec. IV E 2 for $CuGaSe_2$. As can be

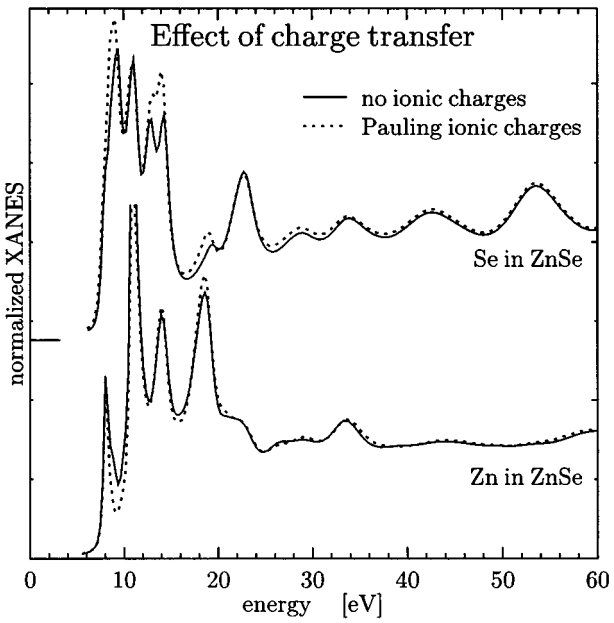

FIG. 9. RS-MS calculation of Zn and Se x-ray-absorption spectra of ZnSe for a cluster of 123 atoms obtained for non-ionic $Zn^{0.00}Se^{0.00}$ (solid line) and for ionic $Zn^{0.57}Se^{-0.57}$ (dotted line) potential models.

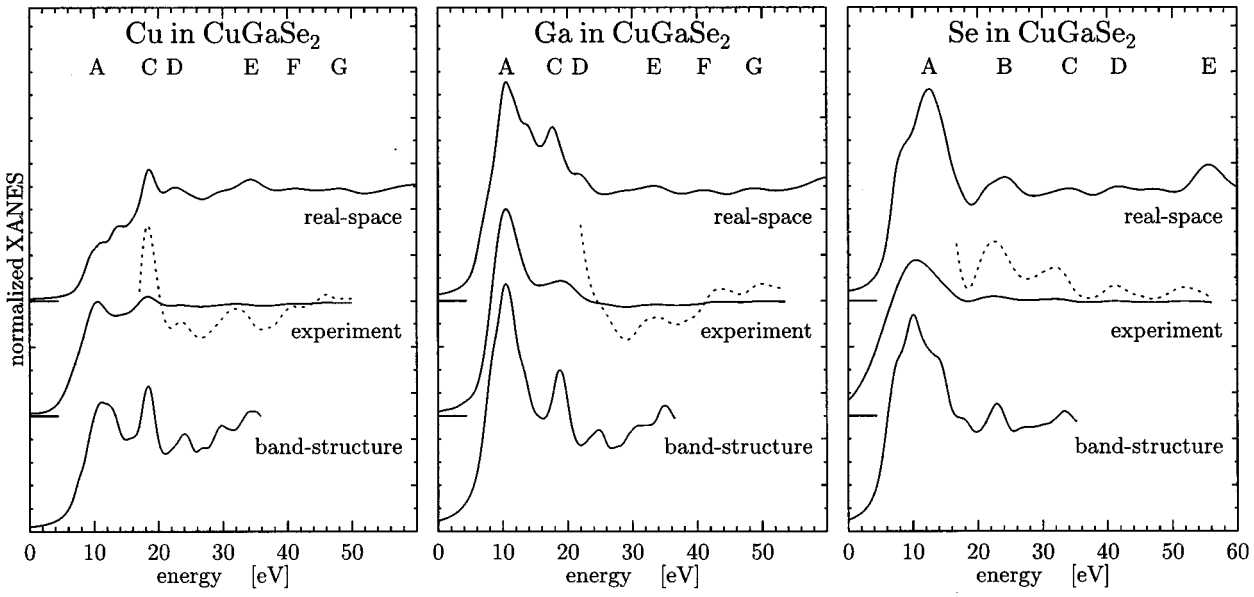

FIG. 10. Experimental and theoretical Cu, Ga, and Se spectra of $CuGaSe_2$. The dotted lines represent experimental curves multiplied by ten. Real-space calculation was performed for clusters of 449 atoms. Core hole was not taken into account. The RS-MS curves were obtained for a muffin-tin version of the self-consistent band-structure potential.

seen from Fig. 10, both RS-MS and band-structure calculations yield theoretical spectra that are in good agreement with experiment—the only exception being failure of the real-space calculation to reproduce peak *A* in the Cu spectrum correctly, as discussed already in Sec. IV D.

For ZnSe, a comparison of theory with experiment is done in Fig. 11. For this compound, real-space calculations were performed for a non-self-consistent Mattheiss potential only. A relaxed and screened core hole was taken into account when calculating the RS-MS curves of Fig. 11, in accordance with the significant core hole effect for Zn spectrum found in Sec. IV E 2. Otherwise, Fig. 11 is analogous to Fig. 10. All features of the experimental curves of Matsuura, Fujikawa, and Oyanagi[5] are reproduced remarkably well by both band-structure and RS-MS calculations, especially where their positions are concerned.

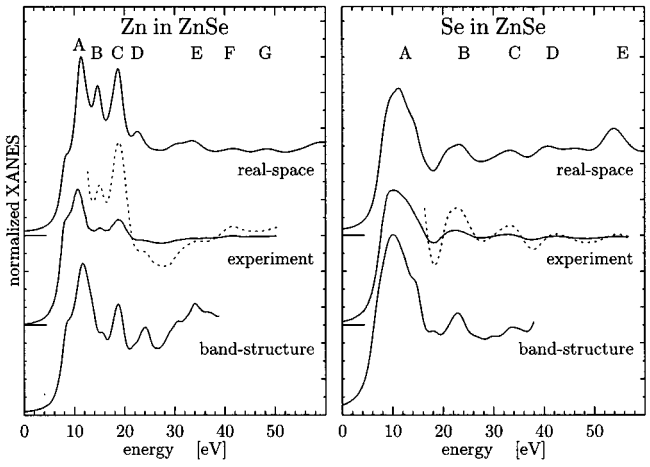

FIG. 11. Experimental and theoretical Zn and Se spectra of ZnSe. The dotted lines represent experiment of Ref. 5 multiplied by ten. Real-space multiple-scattering calculation was performed for clusters of 441 atoms. Non-self-consistent Mattheiss potential with no charge transfer and a relaxed and screened core hole was used for real-space calculations. For band-structure calculations, the core hole was omitted.

Interestingly, although our band-structure calculation did not take into account the core hole, it yields a good ratio for the relative intensity of *A* and *C* peaks of the Zn spectrum—contrary to the case when RS-MS approach was applied to the Mattheiss potential with no core hole (see Fig. 8). This may be due to neglecting the energy dependence of matrix elements in our application of the band-structure formalism, as mentioned in Sec. III A. The influence of matrix elements on x-ray-absorption spectra of semiconductors is currently under investigation (cf. also discussion of possible non-muffin-tin effects in Sec. IV D).

V. CONCLUSIONS

We studied in total five XANES spectra of $CuGaSe_2$ and ZnSe, all corresponding to the same geometrical arrangement of atoms around the absorbing one (different atomic types in nearly identical positions). There are significant differences between cation and anion spectra. The differences between individual edges of the cation group (Cu, Zn, Ga) are larger than differences between the two anion spectra (Se in $CuGaSe_2$ and in ZnSe). We interpret this feature as a manifestation of the role of the chemical type of the absorbing atom. Averaging of formal valences is not directly reflected in XANES spectra—the Zn^{II} spectrum of ZnSe cannot be viewed as just an average of Cu^{I} and Ga^{III} spectra of $CuGaSe_2$.

The experimental spectra of $CuGaSe_2$ and of ZnSe can be described accurately within a one-electron theory both via the band-structure and via the real-space multiple-scattering formalism. The only exception is the first peak in

the Cu spectrum of $CuGaSe_2$, which is correctly accounted for in the band-structure spectrum but is suppressed in the real-space calculation. This may be a consequence of the muffin-tin approximation involved in our RS-MS approach.

In real-space calculation, the most prominent spectral features can be described using clusters of 17 atoms. However, more than 200 atoms are needed to reproduce correctly small peaks as well. For 47-atom clusters, a reasonable agreement between theory and experiment is obtained.

Using self-consistent muffin-tin potential does not lead to significantly better $CuGaSe_2$ spectra than using non-self-consistent Mattheiss potential. Theoretical XANES spectra of $CuGaSe_2$ and ZnSe calculated involving a relaxed and screened core hole are essentially the same as spectra calculated without taking the core hole into account. The largest (and the only significant) core-hole effect was observed for the Zn spectrum of ZnSe. Potentials constructed using relaxed unscreened or unrelaxed unscreened core holes give rise to spectra that are not in agreement with experiment. Employing transfer of charge from cations to anions during Mattheiss potential construction does not lead to important changes in the XANES spectra.

ACKNOWLEDGMENTS

This work was supported by Grant No. 110406 of the Grant Agency of the Academy of Sciences and by Grant No. 202/94/0669 of the Grant Agency of the Czech Republic. The use of the CRYSTIN crystallographic database was supported by the project 203/96/0111 of the Grant Agency of the Czech Republic.

[1] J. E. Jaffe and A. Zunger, Phys. Rev. B **28**, 5822 (1983).
[2] J. Petiau, P. Sainctavit, and G. Calas, Mater. Sci. Eng. B **1**, 237 (1988).
[3] P. Sainctavit *et al.*, Physica B **158**, 623 (1989).
[4] D. A. McKeown, Phys. Rev. B **45**, 2648 (1992).
[5] T. Matsuura, T. Fujikawa, and H. Oyanagi, J. Phys. Soc. Jpn. **53**, 2837 (1984).
[6] See, e.g., W. E. Pickett, Comput. Phys. Rep. **9**, 115 (1989).
[7] J. Vackář and A. Šimůnek, Solid State Commun. **81**, 837 (1992).
[8] G. Bergerhoff, R. Hundt, R. Sievers, and I. D. Brown, J. Chem. Inform. Comput. Sci. **23**, 66 (1983).
[9] A. Šimůnek, M. Polčík, and G. Wiech, Phys. Rev. B **52**, 11 865 (1995).
[10] P. J. Durham, in *X-ray Absorption: Principles, Applications, Techniques*, edited by D. C. Kroningsberger and R. Prins (John Wiley, New York, 1988), p. 53.
[11] D. D. Vvedensky, in *Unoccupied Electron States*, edited by J. C. Fuggle and J. E. Inglesfield (Springer, Berlin, 1992), p. 139.
[12] D. D. Vvedensky, D. K. Saldin, and J. B. Pendry, Comput. Phys. Commun. **40**, 421 (1986).
[13] P. J. Durham, J. B. Pendry, and C. H. Hodges, Comput. Phys. Commun. **25**, 193 (1982).
[14] L. F. Mattheiss, Phys. Rev. **133**, A1399 (1964); **134**, A970 (1964).
[15] Due to lack of space it is not possible to cite all papers demonstrating the usefulness of the Mattheiss potential. A comprehensive list can be found, e.g., in P. Kizler, Phys. Lett. A **172**, 66 (1992).
[16] W. Kohn and L. J. Sham, Phys. Rev. **140**, A1133 (1965).
[17] J. Vackář and A. Šimůnek, J. Phys.: Condens. Matter **6**, 3025 (1994).
[18] B. W. Holland, J. B. Pendry, R. F. Pettifer, and J. Bordas, J. Phys. C **11**, 633 (1978); R. V. Vedrinskii, L. A. Bugaev, and V. M. Airapetian, J. Phys. B **24**, 1967 (1991).
[19] U. von Barth and G. Grossmann, Phys. Rev. B **25**, 5150 (1982).
[20] E. A. Stern and J. J. Rehr, Phys. Rev. B **27**, 3351 (1983).
[21] E. Tamura, J. van Ek, M. Fröba, and J. Wong, Phys. Rev. Lett. **74**, 4899 (1995).
[22] I. Tanaka and H. Adachi, Phys. Rev. B **54**, 4604 (1996).
[23] D. Norman, K. B. Garg, and P. J. Durham, Solid State Commun. **56**, 895 (1985).
[24] R. Gunnella, M. Benfatto, A. Marcelli, and C. R. Natoli, Solid State Commun. **76**, 109 (1990).
[25] C. Li *et al.*, Physica C **175**, 369 (1991).
[26] Th. Lindner, H. Sauer, W. Engel, and K. Kambe, Phys. Rev. B **33**, 22 (1986).
[27] D. G. McCulloch and R. Brydson, J. Phys.: Condens. Matter **8**, 3835 (1996).
[28] R. Zeller, J. Phys. B **72**, 79 (1988).
[29] P. Lerch *et al.*, Phys. Rev. B **45**, 11 481 (1992).
[30] F. Rapisarda and O. Bisi, Phys. Rev. B **47**, 13 914 (1993).
[31] S. Nakai *et al.*, Phys. Rev. B **36**, 9241 (1987).
[32] I. I. Gegusin *et al.*, Phys. Status Solidi B **134**, 641 (1986).
[33] L. T. Wille, P. J. Durham, and P. A. Sterne, J. Phys. (Paris) Colloq. **47**, C8-43 (1986).
[34] X. Weng and P. Rez, Phys. Rev. B **39**, 7405 (1989).
[35] J. C. Phillips, Rev. Mod. Phys. **42**, 317 (1970); R. Burns, *Solid State Physics* (Academic, San Diego, 1985), p. 186.
[36] A. Kisiel *et al.*, Phys. Rev. B **42**, 11 114 (1990).
[37] F. Al Shamma, M. Abbate, and J. C. Fuggle, in *Unoccupied Electron States*, edited by J. C. Fuggle and J. E. Inglesfield (Springer, Berlin, 1992), p. 347.
[38] J. Drahokoupil, I. Drbohlav, J. Horák, M. Polčík, and A. Šimůnek, Solid State Commun. **103**, 303 (1997).
[39] J. Chaboy, Solid State Commun. **99**, 877 (1996).
[40] F. W. Lytle, R. B. Greegor, and A. J. Panson, Phys. Rev. B **37**, 1550 (1988).
[41] O. Šipr, J. Phys.: Condens. Matter **4**, 9389 (1992).
[42] D. L. Foulis, R. F. Pettifer, and P. Sherwood, Europhys. Lett. **29**, 647 (1995); Physica B **208&209**, 68 (1995).
[43] V. N. Datsyuk, I. I. Gegusin, and R. V. Vedrinskii, Phys. Status Solidi B **134**, 175 (1986).
[44] O. Šipr, J. Vackář, and A. Šimůnek, Phys. Rev. B **44**, 4832 (1991).
[45] P. A. Lee, Phys. Rev. B **13**, 5261 (1976).
[46] P. A. Lee and G. Beni, Phys. Rev. B **15**, 2862 (1977).
[47] R. V. Vedrinskii *et al.*, Phys. Status Solidi B **111**, 433 (1982).
[48] P. J. W. Weijs *et al.*, Phys. Rev. B **41**, 11 899 (1990).
[49] M. Kitamura, C. Sugiura, and S. Muramatsu, Solid State Commun. **62**, 663 (1987).